Burgers vector analysis of large area misfit dislocation arrays from bend contour contrast in transmission electron microscope images

2002 J. Phys.: Condens. Matter 14 12767

(http://iopscience.iop.org/0953-8984/14/48/315)

INSTITUTE OF PHYSICS PUBLISHING JOURNAL OF PHYSICS: CONDENSED MATTER

J. Phys.: Condens. Matter **14** (2002) 12767–12776 PII: S0953-8984(02)54081-9

Burgers vector analysis of large area misfit dislocation arrays from bend contour contrast in transmission electron microscope images

E Spiecker and W Jäger

Mikrostrukturanalytik, Technische Fakultät der Christian-Albrechts-Universität zu Kiel, Kaiserstraße 2, D-24143 Kiel, Germany

Received 27 September 2002
Published 22 November 2002
Online at stacks.iop.org/JPhysCM/14/12767

Abstract

A transmission electron microscopy method is described which allows us to determine the Burgers vectors (BVs) of a large number of interfacial misfit dislocations (MDs) in mismatched heterostructures. The method combines large-area plan-view thinning of the sample for creating a strongly bent electron transparent foil with the analysis of the splitting and displacement of bend contours at their crossings with the MDs. The BV analysis is demonstrated for 60° MDs in a low-mismatched SiGe/Si(001) heterostructure. Crossings of various bend contours with the MDs are analysed with respect to their information content for the BV analysis. In future applications the method may be used for analysing such a large number of MDs that a quantitative comparison with x-ray diffraction experiments, especially with data on diffusely scattered x-rays originating from the strain fields around the dislocations, becomes possible.

1. Introduction

In recent years diffuse x-ray scattering has become a valuable tool for the analysis of misfit dislocation (MD) arrays in partially strain relaxed heterostructures [1–5]. Quantitative models are now available which use correlation functions for the description of the spatial distribution of the MDs [6, 7]. For a critical check of these models statistically relevant experimental data on the arrangement and the Burgers vectors (BVs) of the MDs are needed. However, in the interesting range of medium MD densities where the strain fields of the individual dislocations start to overlap [3, 7] x-ray topography can no longer be used for a characterization of the dislocation arrays due to its limited spatial resolution. In this range transmission electron microscopy (TEM) has to be applied for analysing the arrangement and the BVs of the MDs. However, TEM is usually thought to be unadequate for dealing with more than a few dislocations. For the important case of 60° MDs in low-mismatched semiconductor heterostructures an additional complication arises from the fact that the conventional BV

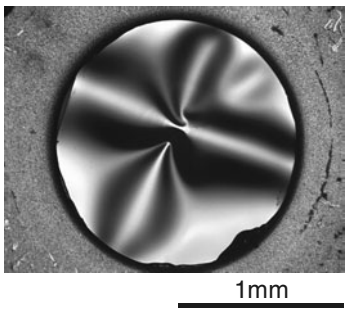

Figure 1. Optical micrograph of the large-area thinned plan-view TEM foil showing the strong foil bending.

analysis based on the simple $\boldsymbol{g} \cdot \boldsymbol{b} = 0$ invisiblility criterion [8] fails due to the presence of pronounced residual contrast in the TEM images. For a determination of the BV the additional condition $\boldsymbol{g} \cdot (\boldsymbol{b} \times \boldsymbol{u}) = 0$ has to be fulfilled which requires considerable tilting of the TEM foil for reaching appropriate excitation conditions [9]. It has been reported that even under these conditions MDs may show residual contrast due to effects of anisotropy or inhomogenity of the elastic medium or due to splitting of the dislocations into partials [10]. Moreover, thin foil bending caused by the epi-layer stress generally leads to a non-uniform dislocation contrast in TEM images making an evaluation over large sample areas tedious. A different approach to the BV analysis of 60° MDs arrays makes use of reactions of dislocations at their mutual crossings [11, 12]. Depending on the combination of the BVs of the crossing MDs characteristic patterns of the dislocation lines are expected to occur. Because there is no unique correspondence between the patterns and the pairs of BVs the informations extracted from several reactions have to be combined for a determination of the BVs. This approach is well-suited for arrays of 60° MDs showing pronounced dislocation reactions. However, in many cases possible reactions of 60° MDs either do not occur or take place over only very short distances making an evaluation of the contrast of crossings ambiguous.

In this paper a new method is described which exploits the effect of foil bending in plan-view TEM samples for the analysis of the BV of interfacial 60° MDs. A large-area thinning procedure is applied in order to extend the foil bending over large sample regions. The BVs of the MDs are determined by evaluation of the splitting and displacement of bend contours at crossings with the MDs in conventional bright-field (BF) or dark-field (DF) images. The method allows us to simultaneously analyse a large number of MDs distributed over a large area of the heterointerface. In contrast to the methods discussed above the complete BV (including the sign!) is obtained.

2. Experimental details

A partially strain-relaxed $Ge_{0.07}Si_{0.93}$/Si(001) heterostructure grown by low-pressure chemical vapour deposition (LPCVD) at 700 °C was used for the present investigation of the BV analysis of 60° MDs. A 3×3 mm^2 piece was cut from the sample and mechanically thinned from the backside to a uniform thickness of $\sim$8 μm using a modified T-tool technique with diamond lapping films [13]. The specimen was glued on a Cu hole grid and further thinned by Ar^+ ion milling (Baltec Res010 system) both from the backside and briefly from the epilayer side in order to obtain a thin foil (50–100 nm in the thinnest parts) with the heterointerface approximately contained in the centre. As a result of this procedure the foil was strongly bent

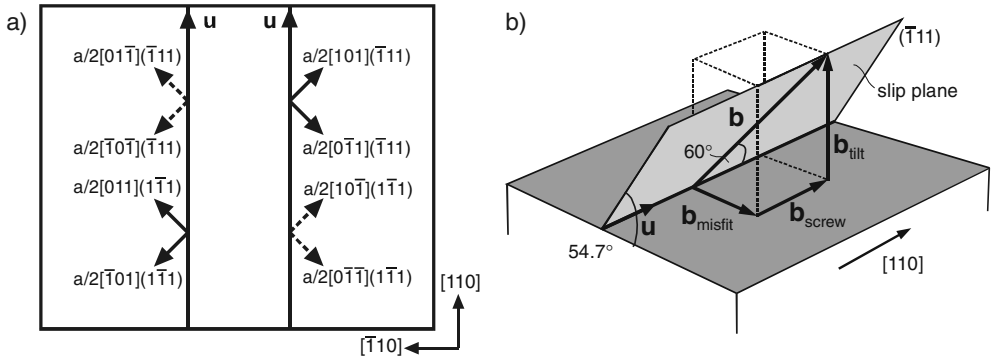

Figure 2. (a) Top view of a SiGe/Si(001), sample showing the eight glide systems of 60° MDs with line direction parallel to [110]. The arrows show the BVs projected onto the (001) plane. Continuous vectors point out of the plane of the paper towards the reader while dashed vectors point into the drawing plane. The four glide systems on the left-hand side contribute to relaxation of tensile layer strain, whereas the four glide systems on the right-hand side contribute to relaxation of compressive layer strain. The BVs are defined according to the FS/RH convention for the Burgers circuit [14]. (b) The BV of one of the 60° MDs decomposed into its three components (see the text).

(figure 1) and contained an electron-transparent region of $\sim 200 \times 200\ \mu m^2$ where the BV analysis could be performed. The specimen was mounted in the stage of a Philips CM30 TEM with the epi-layer normal pointing towards the incident electron beam. The TEM investigation was carried out at an acceleration voltage of 300 kV.

3. 60° misfit dislocations in (001) semiconductor heterostructures

Interfacial 60° MDs in low-mismatched (001) semiconductor heterostructures are aligned along the two orthogonal ⟨110⟩ directions. Apart from polarity effects in the compound semiconductors leading to a discrimination between α- and β-dislocations (see e.g. [9]) the two sets of orthogonal MDs are fully equivalent. In the following we therefore consider only one set of dislocations, namely those with line direction $\boldsymbol{u}$ parallel to [110]. There are four different glide systems of 60° MDs which contribute to the relaxation of compressive layer strain (figure 2(a), right-hand side): $(a/2)[101](\bar{1}11)$, $(a/2)[0\bar{1}1](\bar{1}11)$, $(a/2)[10\bar{1}](1\bar{1}1)$ and $(a/2)[0\bar{1}\bar{1}](1\bar{1}1)$. By changing the sign of the BVs four glide systems are obtained which contribute to the relaxation of tensile layer strain (figure 2(a), left-hand side). Since in semiconductor heterostructures there are indications for the existence of BVs with the 'wrong' sign [11, 15] a BV analysis generally has to discriminate between all eight possible glide systems. In addition, pure edge dislocations with BVs $\pm(a/2)[1\bar{1}0]$ may be formed by reaction of two parallel 60° MDs. However, these dislocations can be easily identified by the invisibility criterion because their contrast completely vanishes under two-beam conditions for $\boldsymbol{g} = 220$ due to $\boldsymbol{g} \cdot \boldsymbol{b} = 0$ and $\boldsymbol{g} \cdot (\boldsymbol{b} \times \boldsymbol{u}) = 0$ [16]. For the BV analysis of the 60° MD it is convenient to describe the BV as being composed of three parts, e.g. $(a/2)[101] = (a/4)[1\bar{1}0] + (a/4)[110] + (a/2)[001] = \boldsymbol{b}_{misfit} + \boldsymbol{b}_{screw} + \boldsymbol{b}_{tilt}$ (figure 2(b)). While the misfit component $\boldsymbol{b}_{misfit}$ generally contributes to the relaxation of the in-plane layer strain, the other two components add strain to the layer: the screw component $\boldsymbol{b}_{screw}$ locally twists the layer crystal around the [001] direction and the tilt component $\boldsymbol{b}_{tilt}$ leads to a local tilt of the [001] direction of the layer relative to the [001] direction of the substrate.

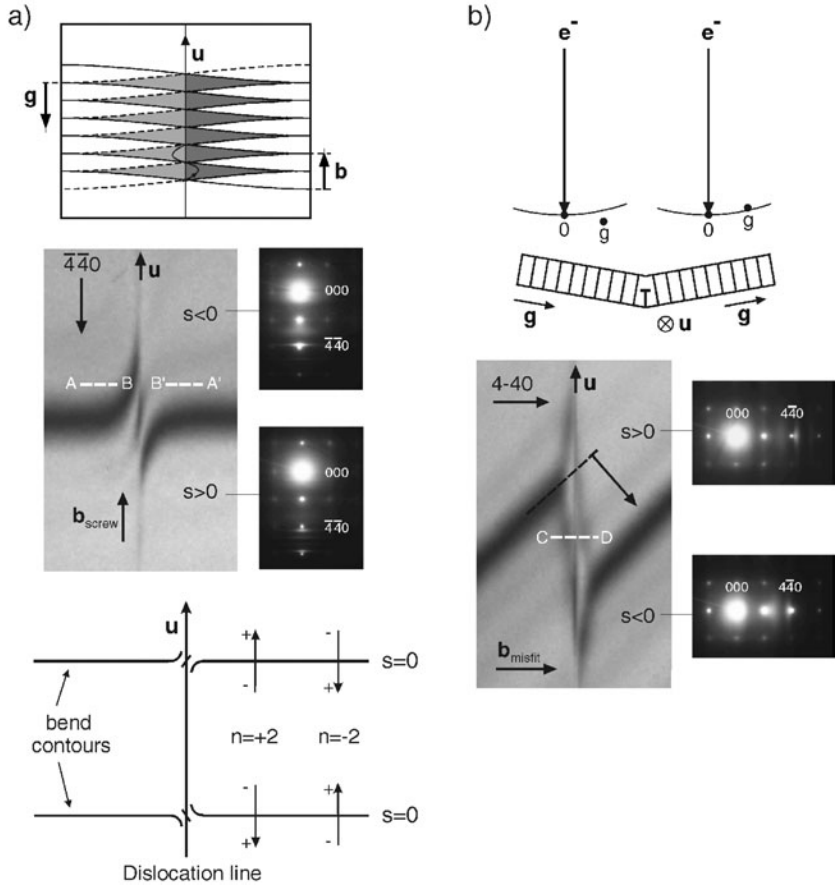

Figure 3. Contrast effects of bend contours at the crossing with a 60° MD running along [110]. (a) The splitting and twisting of the $\bar{4}\bar{4}0$ bend contour can be used for the determination of the screw part $\boldsymbol{b}_{screw}$ of the BV. For the evaluation the rules by Cherns and Preston [12, 13] illustrated in the bottom part can be adopted (see the text). (b) Dislocation induced foil bending leads to a global displacement of the $4\bar{4}0$ bend contour from one side of the dislocation to the other side (see arrow). From the direction of the displacement the sign of the misfit component $\boldsymbol{b}_{misfit}$ of the BV can be determined (see the text).

4. Method: analysis of BVs of 60° MDs

Two contrast effects of bend contours at crossings with the 60° MDs are exploited for the BV analysis:

(i) the twisting and splitting of the bend contour caused by the dislocation strain field, and
(ii) the displacement of the bend contours due to thin-foil bending caused by the misfit component of the BVs.

The evaluation of these contrast effects is illustrated in figures 3(a) and (b), respectively.

Figure 3(a) (centre part) shows a TEM BF image of the $\bar{4}\bar{4}0$ bend contour (horizontal line) crossing a 60° MD with line direction $\boldsymbol{u}$ parallel to [110] (faded vertical line). From the splitting and twisting of the bend contour at the dislocation the value of $\boldsymbol{g} \cdot \boldsymbol{b}$ can be inferred, where $\boldsymbol{g}$ is the reflection related to the bend contour and $\boldsymbol{b}$ is the BV of the dislocation. Cherns

and Preston [17, 18] developed rules for the splitting and twisting of Bragg lines at crossings with dislocations in large-angle convergent-beam electron diffraction (LACBED) images. Due to the analogy between Bragg lines in LACBED images and bend contours in conventional BF images these rules may be applied to bend contours as well [19]. In the lower part of figure 3(a) the rules are illustrated for cases with $n := \boldsymbol{g} \cdot \boldsymbol{b} = \pm 2$. The value of n corresponds to the number of intensity maxima occurring at the splitting in the BF image. The sign of n is related to the direction of the twist of the bend contour near the dislocation relative to the chosen line direction $\boldsymbol{u}$ of the dislocation and the direction in which the excitation error s increases across the bend contour. Several possible combinations and resulting values for n are shown in the drawing. Experimentally, the sign of s on either side of the bend contour may be determined by selected area diffraction (SAD) patterns (figure 3(a), centre part). Applying the rules by Cherns and Preston to the experimental BF image the case $n = -2$ is identified. From $\boldsymbol{g} \cdot \boldsymbol{b} = -2$ the screw part of the BV of the 60° MD is found to be $+(a/4)[110]$. Actually, in order to discriminate between the two possible screw components of the BV, $+(a/4)[110]$ or $-(a/4)[110]$, it is sufficient to identify the direction of the twist of the $\bar{4}\bar{4}0$ bend contour. The origin of the twist can be understood from the drawing in the upper part of figure 3(a) showing the bending of the $\bar{4}\bar{4}0$ lattice planes caused by the screw component of the BV viewed from the direction of the incident electron beam. On the left-hand side of the dislocation the $\bar{4}\bar{4}0$ lattice planes (grey) are rotated towards the electron beam, i.e. the excitation error of the reflection $\bar{4}\bar{4}0$ changes in direction of more positive values ($s\uparrow$). In contrast, on the right-hand side of the dislocation the planes are rotated away from the incident electron beam ($s\downarrow$). In the experimental situation the foil is additionally bent due to global strain in the foil which leads to a continuous change of s from negative values in the upper part of the BF image to positive values in the lower part of the image as revealed by the SAD patterns. Starting now from negative values of s in the bulk (points marked A and A′ in the BF image) the lattice planes are rotated towards the Bragg condition ($s = 0$) when approaching the dislocation from the left-hand side (line A–B in the BF image) whereas the lattice planes bent away from the Bragg condition when approaching the dislocation from the right-hand side (line A′–B′). This explains the corresponding twist of the bend contour near the dislocation and confirms the result $\boldsymbol{b}_{screw} = +(a/4)$ [110].

Figure 3(b) shows in the lower part a BF image of the $4\bar{4}0$ bend contour crossing a 60° MD with line direction $\boldsymbol{u}$ parallel to [110]. Additionally to the localized effect of the strain field of the dislocation on the bend contour contrast leading in this case to a symmetrical splitting of the contour there is a pronounced displacement of the contour from one side of the dislocation to the other side (see arrow). This displacement is due to foil bending caused by the misfit component of the BV as illustrated in the drawing in the upper part of figure 3(b) and can be used for a determination of the sign of $\boldsymbol{b}_{misfit}$. For a general discussion of the effect of dislocation induced foil bending we refer to the textbook by Hirsch *et al* [8] and the references therein. In the drawing figure 3(b) it is assumed that the MD contributes to the relaxation of the compressive SiGe layer strain and therefore the additional lattice plane was inserted from the lower (= substrate) side resulting in the indicated foil bending. The corresponding change of the excitation condition from one side of the dislocation to the other side is schematically illustrated by the drawings of the reciprocal lattice points relative to the Ewald sphere. The excitation error of $\boldsymbol{g} = 4\bar{4}0$ changes more or less abruptly in the positive direction ($s\uparrow$) when crossing the dislocation from left to right. Indeed, along the line C–D in the experimental BF image the excitation error changes from negative to positive values. Therefore the sign of the misfit component of the BV indeed corresponds to relaxation of compressive layer strain as assumed in the drawing, i.e. $\boldsymbol{b}_{misfit} = (a/2)[1\bar{1}0]$ (cf figure 2(a)).

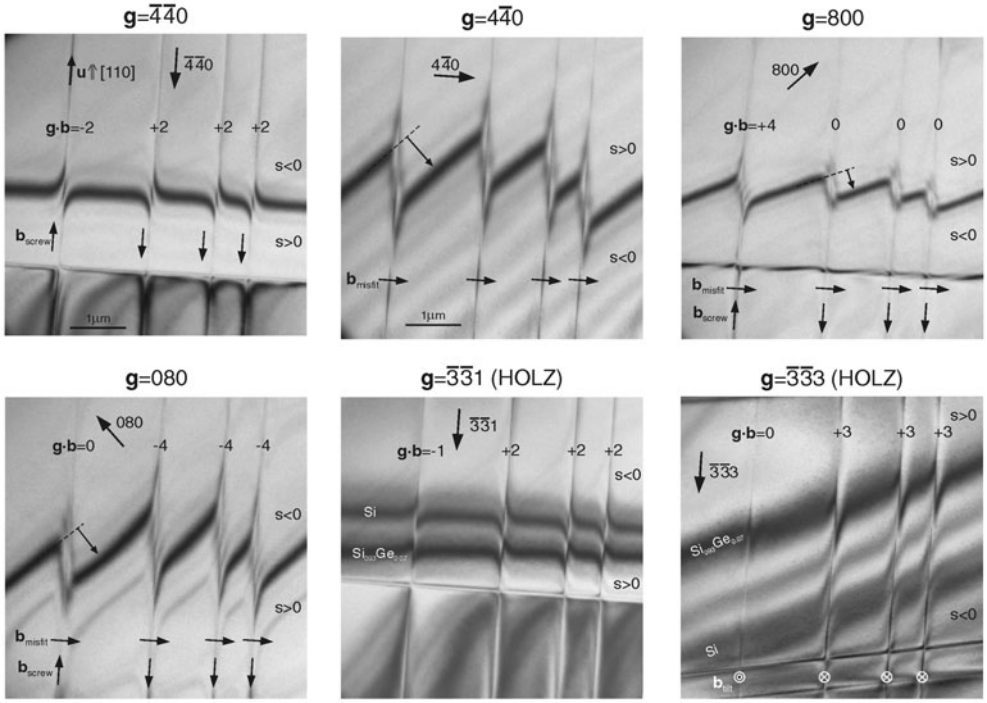

Figure 4. BV analysis of a group of four parallel 60° MDs by analysis of different bend contours (for details, see the text).

For a complete determination of the BVs of the 60° MDs the information of different bend contours has to be combined. In figure 4 BF images of the crossings of various bend contours with a group of four parallel MDs running along [110] are shown. As already discussed in detail above the $\bar{4}\bar{4}0$ and the $4\bar{4}0$ bend contours can be used for the determination of the screw component and the misfit component of the BVs, respectively. The resulting BV components are indicated by arrows in the lower parts of the images. As expected, the misfit components of the four MDs are identical and contribute to relaxation of the compressive SiGe layer strain. By using either the 800 or the 080 bend contours both BV components, $\boldsymbol{b}_{screw}$ and $\boldsymbol{b}_{misfit}$, can be obtained from a single image. As in the case of the $4\bar{4}0$ bend contour the misfit component is determined by the direction of the displacement of the bend contour due to the dislocation induced foil bending. Furthermore, the screw component can be inferred from the bend contour splitting which takes on values $n = 0, \pm 4$. The three cases are easily discriminated. For $n = \pm 4$ corresponding intensity maxima are clearly visible and the sign of n is seen from the direction of the twist of the bend contour. For $n = 0$ disregarding the displacement of the bend contour due to the dislocation induced foil bending the contour splits symmetrically. Numerical simulations of the bend contour splittings based on the dynamical theory of electron scattering and the column approximation reproduce the observed contrast features [20]. Finally, it should be mentioned that it is also possible to determine the two BV components $\boldsymbol{b}_{misfit}$ and $\boldsymbol{b}_{screw}$ without making use of the bend contour displacement caused by the dislocation induced foil bending. For this the analyses of the splittings of either two of the bend contours $\bar{4}\bar{4}0$, 080 and 800 have to be combined.

The more elaborate part of the BV analysis is the determination of the sign of the tilt component $\boldsymbol{b}_{tilt} = \pm(a/2)[001]$. In order to be most sensitive to this BV component bend

contours of higher-order Laue zone (HOLZ) reflections for which $\boldsymbol{g} \cdot \boldsymbol{b}_{tilt} \neq 0$ have to be analysed. The HOLZ bend contours are, however, also sensitive to the tetragonal distortions of the unit cells of the epilayer and the substrate caused by the lattice mismatch. As a result these bend contours split into two lines away from the MDs in coherent regions of the heterostructure (figure 4). This behaviour is analogous to the HOLZ line splitting in convergent beam electron diffraction (CBED) or LACBED from coherently strained heterostructures [18]. At the crossings with the MDs each of the two lines of the HOLZ bend contour shows a splitting which is related to the value of $\boldsymbol{g} \cdot \boldsymbol{b}$ (figure 4). The splitting is not as clearly revealed as in the case of the $\bar{4}\bar{4}0$ bend contour and counting of maxima at the splitting is aggravated. In the case of the bend contour $\bar{3}\bar{3}3$ (figure 4, bottom right) the only possible values for $\boldsymbol{g} \cdot \boldsymbol{b}$ are $n = 0, -3$ and +3 whereby the value $n = -3$ only appears for BV with the 'wrong' sign of the misfit component corresponding to MDs which increase the compressive layer strain rather than decrease it. In the experimental BF image the case $n = 0$ is easily identified from the absence of any splitting (see MDs on the left-hand side of the image). The value $n = +3$ for the other three MDs is found from the direction of the twists of the bend contour lines at the crossings with the MD. This example shows that due to the limited number of possible values for n an explicit counting of the maxima occurring in the splitting region is not always necessary. Dynamical simulations of the Bragg line splittings confirm the correctness of this simplified evaluation [20].

5. Discussion

The method for BV analysis of 60° MDs presented in the last section is based on the evaluation of contrast effects of bend contours at crossings with the dislocations in conventional TEM images. Both effects, the splitting and the displacement of bend contours, may be qualitatively treated within the framework of two-beam diffraction theory (figure 3). The conventional BV analysis based on the invisibility criterion as well makes use of two-beam diffraction theory. What are the differences which make the analysis of bend contours advantageous? Instead of the low-index reflections used in connection with the invisibility criterion the bend contour method makes use of medium- or high-index reflections (cf figure 4). Due to the smaller width of the corresponding bend contours even for moderate foil bending the full range of excitation conditions is covered within a quite small area of the sample. At the crossings with MD the two-beam contrast behaviour is mapped for the complete range of excitation conditions allowing us to perform a reliable contrast analysis (cf figure 3). By tilting the sample in the image mode the bend contours can be shifted across the sample in order to produce crossings with various MDs at different locations. Excitation of a low-index reflection generally results in a more homogenous image contrast even in the case of foil bending. This may be advantageous for the analysis of the arrangement of the MDs. However, for the BV analysis the situation is different. As already mentioned in the introduction the presence of residual contrast poses a problem for the BV analysis of 60° MDs via the invisibility criterion. For a reliable analysis a precise knowledge of the excitation condition is required. An MD which shows faded contrast in one part of the image may give rise to stronger contrast in other parts of the image due to a slight change of the excitation error of the low-index reflection. Because only a small part of the broad bend contour is usually visible in one image the local value of the excitation error cannot be extracted from the image itself but has to be determined separately e.g. by analysis of SAD patterns. Moreover, due to the small extinction distances of low-index reflections dynamical diffraction effects may be important for the BV analysis. In contrast, the effective extinction distances of medium and high-index reflections are generally large compared to the sample thickness. Therefore kinematical theory may be used for a qualitative treatment of the bend contour splitting and displacement.

As already mentioned in the last section there is a close analogy between bend contours in conventional TEM images and Bragg lines in LACBED images. Both types of image can be used for an analysis of the BV of dislocations [19]. To our knowledge the LACBED technique has only been used once for the BV analysis of 60° MDs in semiconductor heterostructures [10]. The Bragg line splitting observed by these authors well agrees with our results on bend contours. In contrast to our work the displacement of Bragg lines due to dislocation induced foil bending was not exploited for the determination of the BVs. The reason for this may be a larger sample thickness used in the LACBED experiments resulting in a reduced effect of dislocation induced foil bending [8, 21]. Generally speaking, LACBED and bend contour imaging are complementary techniques for the analysis of BVs of dislocations. Which technique should be used depends on whether strong bending of the electron transparent foil occurs or not. In the case of plan-view specimens prepared from samples containing strained heterostructures there is an inherent tendency for strong foil bending. Therefore the analysis of bend contours is usually well suited for the BV determination (cf figures 3–5). Reduced foil bending is expected in thicker regions of the TEM sample (cf figure 1) or in cases where the strain in the thin TEM foil is partially balanced by the presence of an appropriate cap layer [19, 22]. Here application of the LACBED technique may be advantageous.

6. Application: large-area Burgers vector analysis of arrays of 60° misfit dislocations

A main advantage of the BV analysis using bend contours is that the method can be applied for a simultaneous determination of the BVs of a large number of dislocations distributed over large sample regions. In order to demonstrate this figure 5 exemplarily shows series of BF images and corresponding $\bar{4}\bar{4}0$ DF images which span a total length of $\sim$100 μm perpendicular to one family of 60° MDs (along [110]) of the two-dimensional dislocation array. Between subsequent images of the series the foil has been sometimes slightly tilted in order to avoid crossings of the bend contours with MD along [$\bar{1}$10]. From the twists of the $\bar{4}\bar{4}0$ bend contour at the crossings with the MDs along [110] the screw parts of the BVs of $\sim$50 dislocations are directly obtained. The resulting screw components of the MDs are indicated by arrows in the DF images. From the frequent change of the sign of the screw component it can already be concluded that pronounced BV bunching does not occur in the sample. Similar series of images (not shown here) were obtained from the other bend contours, such as $4\bar{4}0$, 800, 080 and $\bar{3}\bar{3}3$, and can be used for a complete determination of the BVs of all the 60° MDs contained in figure 5. In an analogous way the BVs of a large number of MDs along [$\bar{1}$10] may be determined. Following this procedure it will be possible to derive for the first time statistically relevant data on the distribution of the MDs among the glide systems for e.g. a quantitative study of the phenomenon of BV bunching and for a quantitative modelling of diffuse x-ray scattering originating from the MDs.

7. Summary and conclusion

A TEM method for the BV analysis of 60° MDs across large areas of the heterostructure has been developed which exploits the splitting and displacement of bend contours in conventional BF or DF images at crossings with the dislocations. In contrast to the commonly used analysis by the invisibility criterion the complete BV (including the sign!) is obtained by our method. Combined with large-area thinning of the TEM plan-view foil the new method allows us to simultaneously analyse the BVs of a large number of MDs distributed over large regions of the sample. Using this method it is be possible to obtain in the range of medium dislocation

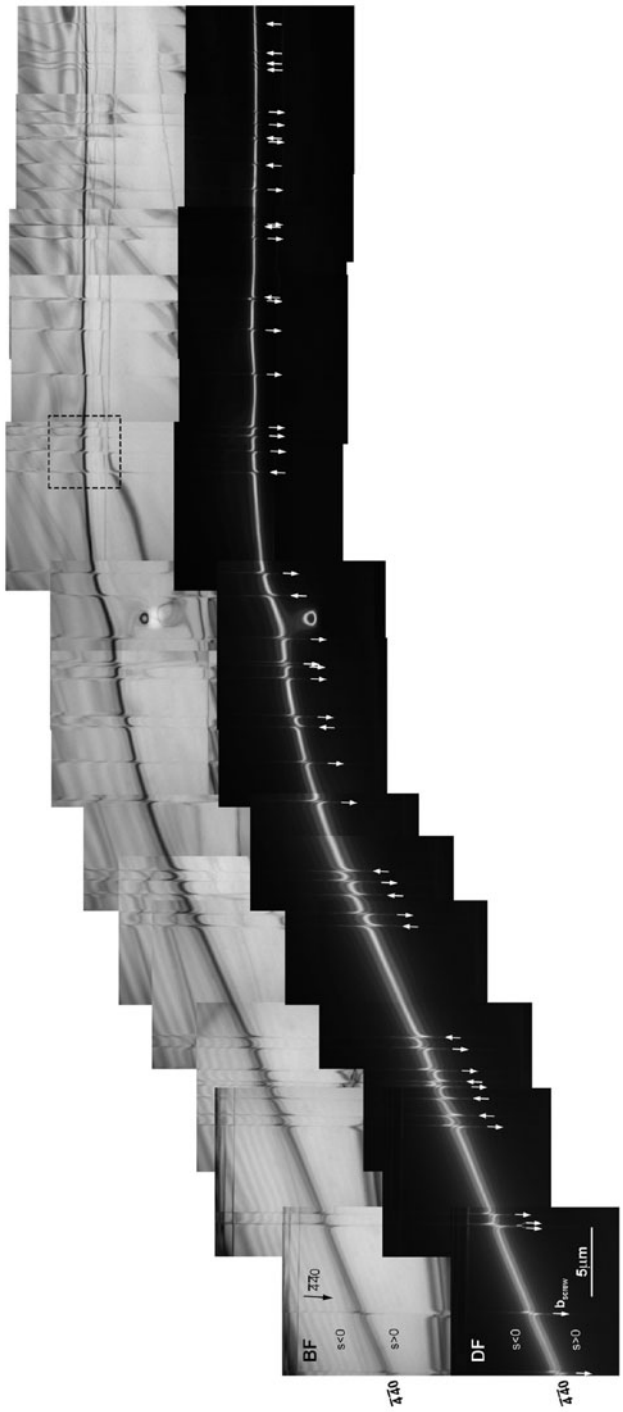

Figure 5. Large-area application of the bend contour method for BV analysis of 60° MDs: determination of the screw parts (see arrows in the DF image) of the BV of ∼50 MDs distributed over ∼100 μm of the Si/SiGe heterointerface.

densities for the first time statistically relevant data on the distribution of the MDs among the glide systems for a quantitative comparison with measurements of diffusely scattered x-rays originating from the dislocations.

Acknowledgments

The authors thank Dr L Vescan (Research Centre Jülich, Germany) for providing the Si/SiGe heterostructure used in this study. They further thank P Rosner (University of Erlangen, Germany) for helpful comments on the T-tool technique.

References

[1] Fewster P 1992 *J. Appl. Crystallogr.* **25** 714
[2] Goorsky M S, Meshkinpour M, Streit D C and Block T R 1995 *J. Phys. D: Appl. Phys.* **28** A92
[3] Lee S R and Floro J A 1996 *Mater. Res. Soc. Symp. Proc.* **399** 455
[4] Großmann V, Heinke H, Leonardi K and Hommel D 2000 *J. Cryst. Growth* **214/215** 447
[5] Barabash R I, Donner W and Dosch H 2001 *Appl. Phys. Lett.* **78** 443
[6] Holý V, Li J H, Bauer G, Schäffler F and Herzog H-J 1995 *J. Appl. Phys.* **78** 5013
[7] Kaganer V M, Köhler R, Schmidbauer M, Opitz R and Jenichen B 1997 *Phys. Rev.* B **55** 1793
[8] Hirsch B, Howie A, Nicholson R B, Pashley D W and Whelan M J 1965 *Electron Microscopy of Thin Crystals* (London: Butterworths)
[9] Herbeaux C, Di Persio J and Lefebvre A 1989 *Appl. Phys. Lett.* **54** 1004
Spiecker E 2002 *Ultramicroscopy* **92** 111
[10] Wang J, Steeds J W and Woolf D A 1992 *Phil. Mag.* A **65** 829
[11] Dixon R H and Goodhew P J 1990 *J. Appl. Phys.* **68** 3163
[12] Beanland R, Kiely C J and Pond R C 1994 *Handbook on Semiconductors* vol 3, 2nd edn, ed T S Moss (Amsterdam: Elsevier) p 1149
[13] Zhang H 1998 *Thin Solid Films* **320** 77–85
The prepration technique described in this article has been modified by P Schubert-Bischoff, Hahn-Meitner Institut, Berlin
[14] Hirth J P and Lothe J 1982 *Theory of Dislocations* (New York: McGraw-Hill)
[15] Matragrano M J, Ast D G, Shealy J R and Krishnamoorthy V 1996 *J. Appl. Phys.* **79** 8371
[16] Fitzgerald E A, Ast D G, Kirchner P D, Peppit G D and Woodall J M 1988 *J. Appl. Phys.* **63** 693
[17] Cherns D and Preston A R 1986 *Proc. 11th Int. Congr. on Electron Microscopy (Kyoto)* vol 1, ed T Imura, S Marusa and T Suzuki (Tokyo: Japan. Soc. Electron Microscopy) p 721
[18] Cherns D and Preston A R 1989 *J. Electron Microsc. Tech.* **13** 111
[19] Morniroli J P 2002 Large-angle convergent-beam electron diffraction (LACBED): application to crystal defects *Monographs of the French Society of Microscopies* Paris
[20] Spiecker E and Jäger W, in preparation
[21] Chou C T, Preston A R and Steeds J W 1992 *Phil. Mag.* **65** 863
[22] Howard D J, Paine D C and Sacks R N 1991 *J. Electon Microsc. Tech.* **18** 117